

## Placing Individual Molecules in the Center of Nanoapertures

Stephan F. Heucke,<sup>†</sup> Fabian Baumann,<sup>†</sup> Guillermo P. Acuna,<sup>‡</sup> Philip M. D. Severin,<sup>†</sup> Stefan W. Stahl,<sup>†</sup> Mathias Strackharn,<sup>†</sup> Ingo H. Stein,<sup>†</sup> Philipp Altpeter,<sup>†</sup> Philip Tinnefeld,<sup>\*,‡</sup> and Hermann E. Gaub<sup>†</sup>

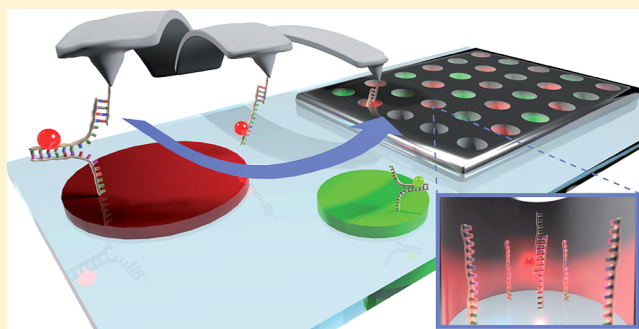
<sup>†</sup>Center for Nanoscience and Department of Physics, University of Munich, Amalienstrasse 54, 80799 Munich, Germany

<sup>‡</sup>Physical and Theoretical Chemistry - NanoBioScience, TU Braunschweig, Hans-Sommer-Strasse 10, 38106 Braunschweig, Germany

### **S** Supporting Information

**ABSTRACT:** While nanophotonic devices are unfolding their potential for single-molecule fluorescence studies, metallic quenching and steric hindrance, occurring within these structures, raise the desire for site-specific immobilization of the molecule of interest. Here, we refine the single-molecule cut-and-paste technique by optical superresolution routines to immobilize single fluorescent molecules in the center of nanoapertures. By comparing their fluorescence lifetime and intensity to stochastically immobilized fluorophores, we characterize the electrodynamic environment in these nanoapertures and proof the nanometer precision of our loading method.

**KEYWORDS:** Nanoapertures, zero-mode waveguides, extraordinary transmission, single-molecule cut-and-paste, single-molecule fluorescence, fluorescence lifetime imaging



Optical spectroscopy of single enzymes provides unique insights into their activity but at the same time requires sophisticated means to cope with the high label concentrations needed. A prominent approach to overcome the concentration limitation is the placement of molecules in zero-mode waveguides (ZMWs).<sup>1,2</sup> These nanoapertures in opaque metallic films have diameters below cutoff, that is, smaller than approximately half the wavelength of the incident light. The resulting strong confinement of the excitation light to an evanescent field at the apertures' bottom results in observation volumes more than 3 orders of magnitude smaller than a diffraction-limited laser focus.<sup>2</sup> With standard nanolithography allowing their mass production,<sup>3</sup> ZMWs became the flagship of commercialized nanophotonic single-molecule technology in their application for single-molecule real-time DNA sequencing.<sup>4</sup> The fast and unambiguous optical read-out of single ligand binding events also led to the direct observation of translation,<sup>5</sup> protein–protein interactions<sup>6</sup> and even allowed epigenetic DNA sequencing.<sup>7</sup>

In all of these studies, enzymes were immobilized from solution resulting in a low yield of ZMWs with only one immobilized enzyme. By this stochastic immobilization, single-occupation can be maximized to a theoretical Poissonian limit of only 37%.<sup>8</sup> In addition, the fluorescence signal intensities are expected to vary strongly, due to the randomly distributed distances of the immobilized enzymes to the fluorescence quenching metallic sidewalls. This further reduces the fraction of ZMWs that can be used for analysis as well as quantitative spectroscopic measurements of biomolecular processes.

Here, we investigated this anisotropy by placing single fluorescent molecules in ZMWs first in a stochastic and then in a controlled manner. We refined the recently developed single-molecule cut-and-paste technique (SMC&P)<sup>9</sup> by superresolution routines for pasting individual fluorophores into the center of nanoapertures. The greatly reduced heterogeneity compared to stochastic immobilization demonstrates the nanometer accuracy of our technique while additionally providing a first picture of spatial differences in the electrodynamic environment of zero-mode waveguides.

To characterize the fluorescence properties of individual fluorophores in nanoapertures, single-molecules of double-stranded DNA labeled with one ATTO647N dye were stochastically immobilized in the nanoapertures in a first set of experiments using passivated metal walls and biotin-neutravidin interaction on the bottom of the nanoapertures<sup>4,8</sup> (Figure 1a and Supporting Information). By confocal fluorescence lifetime imaging,<sup>10</sup> we quantified fluorescence intensities and fluorescence lifetimes. Figure 1b shows a false-color fluorescence image of single molecules in 150 nm nanoapertures. In an additional background channel, shown in green, we recorded reflection from the metal cladding and leakage through the dichroic filter to make nanoapertures visible as a dim regular grid. The red spots of different intensity in some of the nanoapertures represent fluorescence from immobilized DNA molecules labeled with ATTO647N. The

**Received:** April 26, 2013

**Revised:** May 29, 2013

**Published:** June 6, 2013

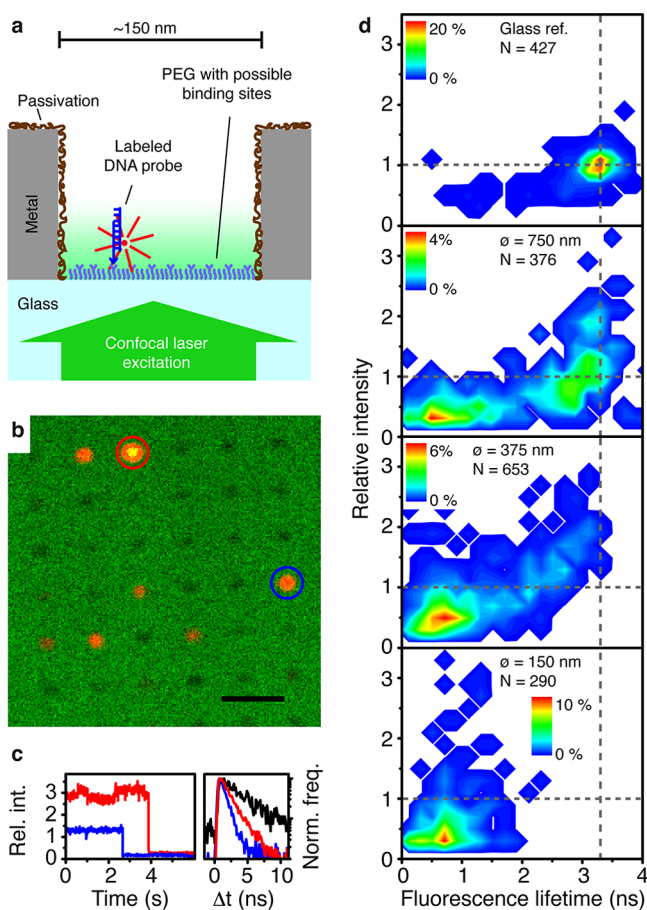


**Figure 1.** Fluorescence heterogeneity from stochastic immobilization. (a) Schematics of the experiment. Dye-labeled double-stranded DNA from solution is immobilized via biotin–avidin binding on a polyethylene glycol (PEG) layer that is restricted to the aperture's bottom by chemical passivation. (b) A false color confocal microscopy image of an array of ZMWs with diameters of 150 nm. The black bar represents 2 μm. ZMWs are visible as dark minima in a background channel (green). A low overall occupation density of the dyes (red), together with single-step bleaching in fluorescence transients assures single-dye occupation of the ZMWs. (c) Transients and fluorescence decay times  $\Delta t$  are plotted for two exemplary dyes (red and blue circles in b). The intensity of the transients is normalized to the mean intensity of a population of reference dyes that were immobilized in a large glass window without metal. For comparison, the fluorescence decay time of one reference dye is graphed in black. (d) Lifetime and intensity data from  $N$  number of dyes immobilized in a large glass reference window and in different diameter apertures are plotted in probability maps. Dyes in apertures reveal pronounced heterogeneity in fluorescence lifetime and an up to 3-fold intensity enhancement compared to dyes immobilized on a glass reference. The longest fluorescence lifetime measured decreases for smaller nanoapertures.

density of fluorophores was kept low to reduce the probability of multiple occupancies. Additionally, single-step photobleaching in fluorescent transients recorded for the brightest spots, such as those depicted in Figure 1c, confirmed that the fluorescence, indeed, can be ascribed to single fluorophores. The different intensity of the fluorescent spots already suggests substantial heterogeneity. This is further characterized in probability density maps correlating fluorescence intensity and fluorescence lifetime of more than 1700 dyes immobilized in different size nanoapertures and on a glass reference surface (Figure 1d). For all nanoapertures, the fluorescence lifetime

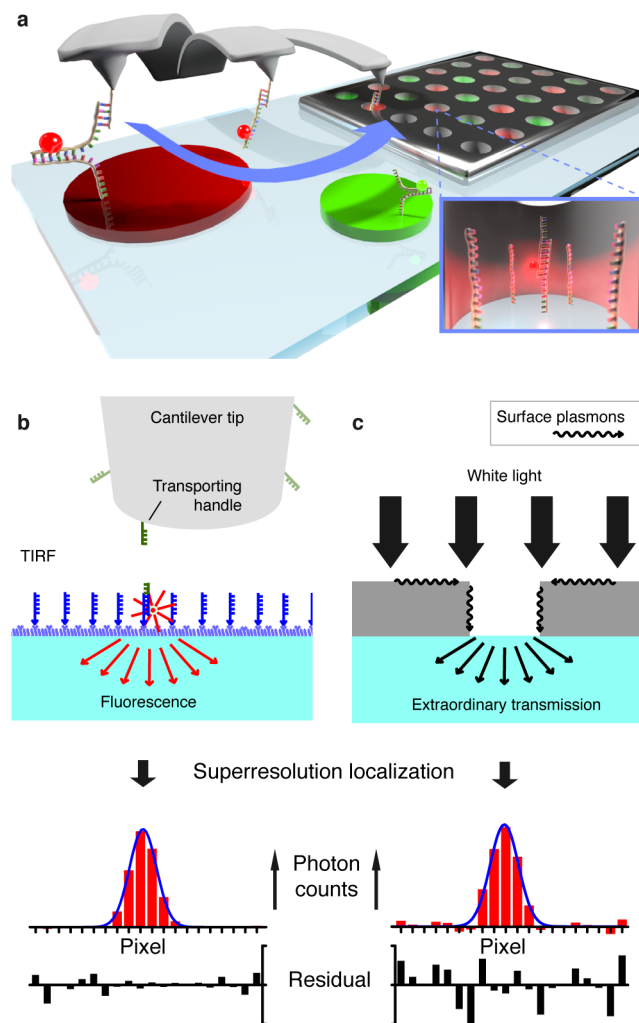


**Figure 2.** (a) Schematics of single-molecule cut-and-paste into nanoapertures. An AFM cantilever is used to transport labeled DNA anchors from a remote depot area into the center of a nanoaperture. (b) The position of the AFM's transporting handle is localized by fitting Gaussians to the fluorescence of a pasted anchor in TIRF microscopy mode. (c) Similarly, white light extraordinarily transmitted through the nanoaperture by surface plasmons is used to localize the apertures by Gaussian fitting of the intensity distribution.

was shorter than that of the glass reference. For all aperture sizes, a population of strongly quenched fluorescence lifetimes close to the time resolution of the setup is observed which extends to longer lifetimes to a degree that depends on the nanoaperture size. Interestingly, the fluorescence intensity normalized to the mean fluorescence intensity of the glass reference (termed relative intensity) is not proportionally correlated with the fluorescence lifetime. While the spots with the short lifetimes exhibit weak fluorescence, some of the molecules with intermediate lifetimes display even stronger fluorescence than the glass reference. The interaction between fluorophores and metallic structures has been theoretically studied for simple geometries such as mirrors<sup>11</sup> and spheres,<sup>12</sup> whereas for more complex geometries such as nanoapertures numerical simulations have been employed.<sup>1,13</sup> Metals can modify all defining rates of a fluorophore (i.e., excitation, radiative, and nonradiative) leading to an enhancement or to a reduction of the fluorescence intensity.<sup>10</sup> Metals generally shorten the fluorescence lifetime, particularly in close vicinity to

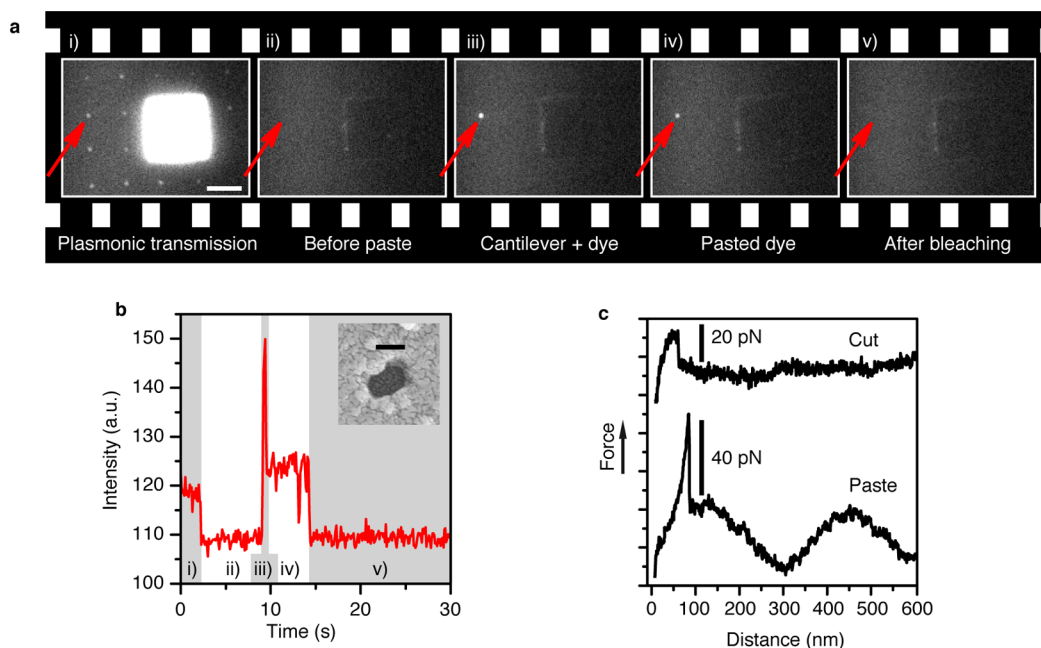


**Figure 3.** Single dyes placed in nanoapertures with SMC&P. (a) Video frames documenting the pasting of a single dye into a 130 nm nanoaperture and (b) the corresponding intensity transient from the aperture show the following five phases: (i) first, extraordinary transmission reveals the position of the aperture about to be loaded (red arrow). (ii) Before the pasting event transmitted light is switched off and none of the nanoapertures show fluorescence under TIRF illumination. (iii) Scattered light from the cantilever tip and dye fluorescence mark the pasting event. (iv) After the cantilever has retracted, the fluorescence signal of a single dye remains before it bleaches in one step bringing the intensity back to background level (v). The inset in the intensity transient is a SEM-image of the actual nanoaperture loaded (bar = 100 nm). The white bar in frame (i) represents 3  $\mu\text{m}$ . (c) Force curves recorded during the cut-and-paste processes show characteristic one-step zipper- (cut) and shear-force (paste) rupturing, respectively. The sine superimposing the paste force curve originates from interference of the AFM's IR-laser with the reflective metal surrounding the ZMW.

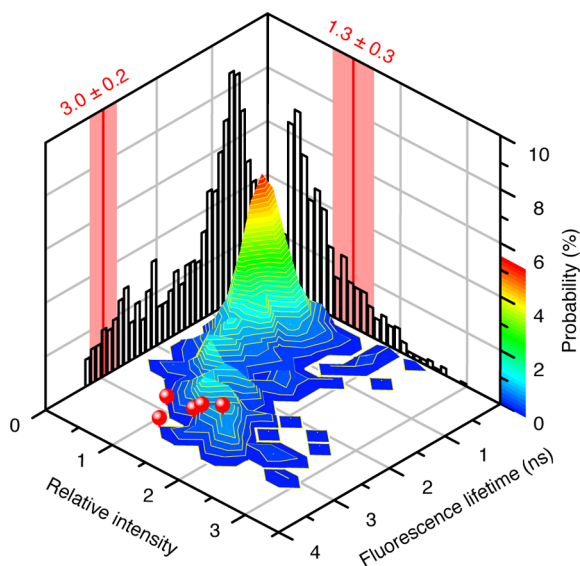


**Figure 4.** Comparison of SMC&P-placed and stochastically immobilized dyes. The lifetimes and relative intensities of the 653 dyes stochastically immobilized in nanoapertures of 375 nm from Figure 1d are presented in a 3D probability plot with corresponding histograms (black). In contrast to these broad distributions of lifetime and relative intensity, five dyes pasted into the center of same-size nanoapertures are confined to long lifetimes and enhanced relative intensity (each red ball represents one pasted dye). Their mean and standard deviation are represented by the red lines and boxes in the histograms.

the metallic surface where the increase of the nonradiative rate prevails.<sup>14</sup> Fluorescence enhancement was, for example, reported for dyes diffusing through nanoapertures in gold<sup>15</sup> and in aluminum films,<sup>16</sup> but little information<sup>17</sup> on spatial distributions or correlation of lifetime and intensity was reported.

In order to overcome the heterogeneity and to assign the fluorescence lifetimes to positions in the nanoapertures, we adapted atomic force microscopy (AFM) based SMC&P<sup>9</sup> to the needs of placing into nanoapertures. We used the cantilever of an AFM as a nanoscopic robotic arm for loading nanoapertures and DNA oligos as programmable handles and anchors (see Figure 2a). In previous studies, single molecules such as DNA,<sup>9,18</sup> avidin binding sites,<sup>19</sup> functional aptamers,<sup>20</sup> or whole proteins<sup>21</sup> were deposited with a precision relative to one another of  $\sim 11$  nm.<sup>18</sup> This approach should not only overcome the Poissonian occupation limit but should also enable signal homogenization and maximization by restricting molecule immobilization to the nanoapertures' center.

A prerequisite for pasting molecules into nanoapertures is to align both the position of the handle DNA oligo on the AFM tip and the position of the nanoapertures with the microscope optics. Since the functionalization of the AFM cantilever tip is a stochastic process where only the functionalization density is controlled and kept within the Poisson limit, those cantilevers are selected that have one active handle only. This is done by monitoring the number of rupture events in the force-traces recorded during SMC&P processes and discarding of cantilevers that show more than one rupture event. To then localize the one active handle oligo whose position on the AFM tip is not known a priori, we first picked up an individual DNA oligo

with its fluorophore from the depot area and then pasted it in a large reference window next to the nanoapertures. Its localization by Gaussian fitting the point-spread function yields the position of the active SMC&P handle on the AFM tip in the coordinate system of the optical microscope with the precision of a few nanometers<sup>22</sup> (Figure 2b). To localize the target nanoaperture, we made use of extraordinary transmission through the subwavelength apertures, a phenomenon first discovered by Ebbesen and co-workers.<sup>23</sup> The transmitted light allows localization of the aperture by a Gaussian fit to its intensity distribution (Figure 2c). Since both positions are defined by this procedure with nanometer precision in the coordinate system of the optical microscope, individual DNA oligos may now be pasted at the bottom of the nanoapertures. In contrast to AFM topography scans used in earlier studies,<sup>24</sup> this procedure is fast and noninvasive since it does not impair the activity of the handle DNA on the cantilever through mechanical contact. The lateral precision of our method was determined to be 19 nm (see Supporting Information for a detailed error analysis).

The detected light intensity during the loading of a 130 nm nanoaperture is shown in Figure 3a,b (see also Supporting Information Supplementary Movie). Initially, the targeted nanoaperture (red arrow) has been aligned with the AFM and is visible by transmitted white light. After the white light is switched off the nanoaperture is loaded with a single DNA strand. The high signal at the beginning of the paste event (stage iii) originates from inelastic scattering of the cantilever's tip.<sup>18</sup> After it is withdrawn, fluorescence from the DNA strand's label remains until it bleaches in a single step. In combination with the single rupture event in the simultaneously recorded force curve of the paste (Figure 3c), this single photobleaching step proves single-molecule occupancy.<sup>9,25</sup> Assuming 100% interaction efficiency and minimized fluorescence acquisition times, the duration of one loading cycle is limited by the traveling and pulling speeds of the AFM to about 3 s. Here, a loading cycle includes the pick-up of a single molecule, its transport to the aperture, fluorescence controlled pasting into the aperture, and subsequent return of the cantilever to the depot. It should be noted here that after bleaching of the label, the pasted DNA strand may be used as anchor point for other molecules of interest in the center of the nanoaperture.

Besides the abilities of total internal reflection fluorescence (TIRF) imaging for synchronization and SMC&P, our setup incorporates a confocal microscope for fluorescence lifetime imaging. This enabled us to carry out SMC&P, to visualize successful pasting in the nanoapertures, and to subsequently switch to the confocal mode for single-molecule spectroscopy of the same molecules. We extracted the fluorescence lifetime by reconvoluting with the instrument response function and quantify the fluorescence intensities by normalizing to the intensities of dye molecules pasted in metal free areas (see Supporting Information for experimental section).

With this protocol, individual fluorophores were pasted into nanoapertures of 375 nm diameter. Fluorescence lifetimes were found in a range around 3 ns close to the maximum of the distribution obtained by stochastic immobilization (see Figure 4, red data points). The narrow fluorescence lifetime distribution suggests that all molecules are successfully pasted close to the center of the nanoapertures. Furthermore, the lifetime of  $\sim 3$  ns in the center of the nanoapertures is consistent with the interpretation that the central region experiences least quenching. Interestingly, the fluorescence

intensity is mostly higher than that of the glass reference in accordance with the distribution of stochastically immobilized molecules (see Figure 4).

Our study shows that stochastic immobilization of molecules in nanoapertures results in a pronounced heterogeneity of fluorescence properties with a high fraction of strongly quenched molecules. We advanced single-molecule cut-and-paste technology to overcome these limitations using a superresolution-based optical navigation technique. Analysis of quantitative confocal single-molecule imaging revealed that the brightest molecules are found near the center of the nanoapertures and that quenching scales with the proximity of the metal walls. Our data indicate that targeted placing of single molecules in nanoapertures, using an approach that is not Poisson-limited, is a key for optimizing single-molecule spectroscopy in nanoapertures. Although the presented serial loading technique might not be time- and cost efficient enough for loading massively parallel assays (thousands of ZMWs) for commercial purposes, the possibility to directly immobilize, for example, different enzyme mutants in neighboring ZMWs brings about new benefits also for moderate numbers of parallel single-molecule assays. Additionally, the site-specific one-by-one immobilization of single molecules can generally facilitate probing of the electromagnetic environment of other nanostructures such as the coupling of optical emitters to antennas.<sup>26</sup>

## ■ ASSOCIATED CONTENT

### Supporting Information

The movie underlying Figure 3a and details of material and methods such as sample fabrication and preparation, AFM cantilever preparation, microscope setups, SMC&P procedure, and a discussion of the method's lateral uncertainty. This material is available free of charge via the Internet at <http://pubs.acs.org>.

## ■ AUTHOR INFORMATION

### Corresponding Author

\*E-mail: [p.tinnefeld@tu-bs.de](mailto:p.tinnefeld@tu-bs.de). Fax: +49 531 391 5334. Phone: +49 531 391 5330.

### Author Contributions

The manuscript was written through contributions of all authors. All authors have given approval to the final version of the manuscript.

### Notes

The authors declare no competing financial interest.

## ■ ACKNOWLEDGMENTS

The authors would like to thank P. Holzmeister, A. Meindl, S. Schneider, A. Vetter, and W. Summerer for technical support and C. Hohmann for artwork. This work was supported by the Volkswagen Stiftung, the German Science Foundation (SFB 863) and the German excellence initiative via the "Nano-systems Initiative Munich" (NIM). S.H. is grateful to the Elite Network of Bavaria (IDK- NBT) for a doctoral fellowship.

## ■ REFERENCES

- (1) Levene, M. J.; Korlach, J.; Turner, S. W.; Foquet, M.; Craighead, H. G.; Webb, W. W. *Science* **2003**, *299* (5607), 682–686.
- (2) Zhu, P.; Craighead, H. G. *Annu. Rev. Biophys.* **2012**, *41* (1), 269–293.

(3) Foquet, M.; Samiee, K. T.; Kong, X.; Chauduri, B. P.; Lundquist, P. M.; Turner, S. W.; Freudenthal, J.; Roitman, D. B. *J. Appl. Phys.* **2008**, *103* (3), 034301.

(4) Eid, J.; Fehr, A.; Gray, J.; Luong, K.; Lyle, J.; Otto, G.; Peluso, P.; Rank, D.; Baybayan, P.; Bettman, B.; Bibillo, A.; Bjornson, K.; Chaudhuri, B.; Christians, F.; Cicero, R.; Clark, S.; Dalal, R.; Dewinter, A.; Dixon, J.; Foquet, M.; Gaertner, A.; Hardenbol, P.; Heiner, C.; Hester, K.; Holden, D.; Kearns, G.; Kong, X.; Kuse, R.; Lacroix, Y.; Lin, S.; Lundquist, P.; Ma, C.; Marks, P.; Maxham, M.; Murphy, D.; Park, I.; Pham, T.; Phillips, M.; Roy, J.; Sebra, R.; Shen, G.; Sorenson, J.; Tomaney, A.; Travers, K.; Trulson, M.; Vieceli, J.; Wegener, J.; Wu, D.; Yang, A.; Zaccarin, D.; Zhao, P.; Zhong, F.; Korlach, J.; Turner, S. *Science* **2009**, *323* (5910), 133–138.

(5) Uemura, S.; Aitken, C. E.; Korlach, J.; Flusberg, B. A.; Turner, S. W.; Puglisi, J. D. *Nature* **2010**, *464* (7291), 1012–1017.

(6) Miyake, T.; Tanii, T.; Sonobe, H.; Akahori, R.; Shimamoto, N.; Ueno, T.; Funatsu, T.; Ohdomari, I. *Anal. Chem.* **2008**, *80* (15), 6018–6022.

(7) Flusberg, B. A.; Webster, D. R.; Lee, J. H.; Travers, K. J.; Olivares, E. C.; Clark, T. A.; Korlach, J.; Turner, S. W. *Nat. Methods* **2010**, *7* (6), 461–465.

(8) Korlach, J.; Marks, P. J.; Cicero, R. L.; Gray, J. J.; Murphy, D. L.; Roitman, D. B.; Pham, T. T.; Otto, G. A.; Foquet, M.; Turner, S. W. *Proc. Natl. Acad. Sci. U.S.A.* **2008**, *105* (4), 1176–1181.

(9) Kufer, S. K.; Puchner, E. M.; Gumpp, H.; Liedl, T.; Gaub, H. E. *Science* **2008**, *319* (5863), 594–596.

(10) Acuna, G. P.; Moller, F. M.; Holzmeister, P.; Beater, S.; Lalkens, B.; Tinnefeld, P. *Science* **2012**, *338* (6106), 506–510.

(11) Drexhage, K. H. *Prog. Optics* **1974**, *12*, 163–232.

(12) Gersten, J.; Nitzan, A. *J. Chem. Phys.* **1981**, *75* (3), 1139–1152.

(13) Fore, S.; Yuen, Y.; Hesselink, L.; Huser, T. *Nano Lett.* **2007**, *7* (6), 1749–1756.

(14) Anger, P.; Bharadwaj, P.; Novotny, L. *Phys. Rev. Lett.* **2006**, *96* (11), 113002.

(15) Wenger, J.; Gerard, D.; Dintinger, J.; Mahboub, O.; Bonod, N.; Popov, E.; Ebbesen, T. W.; Rigneault, H. *Opt. Express* **2008**, *16* (5), 3008–3020.

(16) Wenger, J.; Cluzel, B.; Dintinger, J.; Bonod, N.; Fehrembach, A. L.; Popov, E.; Lenne, P. F.; Ebbesen, T. W.; Rigneault, H. *J. Phys. Chem. C* **2007**, *111* (30), 11469–11474.

(17) Choy, J. T.; Hausmann, B. J. M.; Babinec, T. M.; Bulu, I.; Khan, M.; Maletinsky, P.; Yacoby, A.; Lončar, M. *Nat. Photonics* **2011**, *5* (12), 738–743.

(18) Kufer, S. K.; Strackharn, M.; Stahl, S. W.; Gumpp, H.; Puchner, E. M.; Gaub, H. E. *Nat. Nanotechnol.* **2008**, *4* (1), 45–49.

(19) Puchner, E. M.; Kufer, S. K.; Strackharn, M.; Stahl, S. W.; Gaub, H. E. *Nano Lett.* **2008**, *8* (11), 3692–3695.

(20) Strackharn, M.; Stahl, S. W.; Puchner, E. M.; Gaub, H. E. *Nano Lett.* **2012**, *12* (5), 2425–2428.

(21) Strackharn, M.; Pippig, D. A.; Meyer, P.; Stahl, S. W.; Gaub, H. E. *J. Am. Chem. Soc.* **2012**, *134*, 15193–15196.

(22) Thompson, R. E.; Larson, D. R.; Webb, W. W. *Biophys. J.* **2002**, *82* (5), 2775–2783.

(23) Ebbesen, T. W.; Lezec, H. J.; Ghaemi, H. F.; Thio, T.; Wolff, P. A. *Nature* **1998**, *391* (6668), 667–669.

(24) Heucke, S. F.; Puchner, E. M.; Stahl, S. W.; Holleitner, A. W.; Gaub, H. E.; Tinnefeld, P. *Int. J. Nanotechnol.* **2013**, *10* (5/6/7), 607–619.

(25) Ulbrich, M. H.; Isacoff, E. Y. *Nat. Methods* **2007**, *4* (4), 319–321.

(26) Novotny, L.; van Hulst, N. *Nat. Photonics* **2011**, *5* (2), 83–90.

## Supplementary information

# Placing individual molecules in the center of nanoapertures

**Stephan F. Heucke<sup>1</sup>, Fabian Baumann<sup>1</sup>, Guillermo P. Acuna<sup>2</sup>, Philip M. D. Severin<sup>1</sup>, Stefan W. Stahl<sup>1</sup>, Mathias Strackharn<sup>1</sup>, Ingo H. Stein<sup>1</sup>, Philipp Altpeter<sup>1</sup>, Philip Tinnefeld<sup>2\*</sup> & Hermann E. Gaub<sup>1</sup>**

<sup>1</sup> Center for Nanoscience and Department of Physics, University of Munich, Amalienstrasse 54, 80799 Munich, Germany

<sup>2</sup> Physical and Theoretical Chemistry - NanoBioScience, TU Braunschweig, Hans-Sommer-Strasse 10, 38106 Braunschweig, Germany

\* e-mail: p.tinnefeld@tu-bs.de

## Lithography of nanoapertures

For loading nanoapertures via SMC&P, samples have to contain nanoapertures, a glass window for the depot area as well as a second, smaller glass window for the reference pastes – all within reach of the AFM cantilever. Fig. S1 depicts the structural arrangement used in the underlying experiments. Samples were fabricated with negative e-beam lithography based on a method described in ref. 1. However, we used an alternative photoresist and a discharge layer consisting of silver instead of gold:

**Initial cleaning:** Conventional borosilicate glass cover slips were first cleared from glass debris by a nitrogen stream and then excessively cleaned in solvents: They were immersed in an ultrasonic (US) bath (Super Digital, Bandelin Sonorex) of 2% Hellmanex at 50 °C for 15 min followed by a rinse with water (all water used during lithography was purified and of HPLC grade), a 15 min US-bath in water and again another water rinse to wash away any Hellmanex remains. Further subsequent 15 min US-baths in acetone, isopropanol and water additionally assured removal of any organic contaminations. Finally, samples were again rinsed in water and then dried under a nitrogen stream.

**Photoresist coating:** To increase hydrophobicity of the glass surface, and thus promote photoresist adhesion, the cover slips were treated with an oxygen plasma (GigaEtch, PVA TePla Technics) at 200

W for 180 s and heated up to 120 °C on a hot plate for 120 s. To prevent resorption of air humidity the cover slips were then taken from the hot plate and directly placed onto a spin coater (WS-400-6NPP/LITE/IND, Laurell) where resist promoter (1:10, isopropanol : Ti-Prime, MicroChemicals) was spun onto the samples immediately. Spin coater settings were 4000 rpm for 40 s with a 3 s acceleration ramp of 800 rpm. Primer solvents were evaporated by baking the sample on a hot plate at 120 °C for 120 s. Now photoresist (ma-N 2403, Microresist) was spun onto the sample for 30 s with a 3 s ramp of 800 rpm and a final rotational speed of 3000 rpm followed by a bake at 90 °C for 60 s.

**Deposition of the discharge layer:** To avoid charge accumulations in the nonconducting glass substrate, a 5 nm Ag film was thermally evaporated onto the photoresist from a tungsten boat in a hybrid evaporator (Bestec) capable of e-beam and thermal evaporation. A current of 190 A at a voltage of 0.8 V resulted in a rate of 1.2 Å/s while pressure was  $5 \times 10^{-9}$  mbar prior to evaporation. The samples were water-cooled via physical contact on their backside to prevent heating above the critical cross-linking temperature of the photoresist resin. When evaporating Cr, Au or Al instead, we experienced cross-linking which we denote to the increased thermal radiation coming with the higher boiling points of these metals. To avoid fluctuations in oxidation degree of the Ag discharge layer, samples were transferred into the electron microscope immediately after evaporation.

**Exposure:** Electron beam exposure was made in an eLine system (Raith) with thermal field-emitting cathode (Schottky emitter). An acceleration voltage of 10 kV and an aperture of 20 μm resulted in a beam current of 0.074 nA. Working distance was 8 mm. Apertures with diameters smaller than 150 nm were written as single dots with a dose of 0.023 pC. Apertures with diameters of 150 nm, 375 nm and 750 nm were written as filled circles with a step size of 12.8 nm, a dose of 10 μC/cm<sup>2</sup>. Glass windows were written with a step size of 10 nm and an area dose of 7 μC/cm<sup>2</sup>.

**Development:** Samples were then heated in a post exposure bake at 72 °C on a hot plate for 120 s to increase linking of the exposed photoresist. The discharge layer was dissolved by a 7 s bath in a commercial etchant (Iodine / Potassium iodide = I<sub>2</sub>/KI, 50% aq., Alfa Aesar) followed by a stop and a rinse bath in water for 30 s each. The samples were then developed under slight stirring in ma-D 525 (Microresist) for 70 s, stopped from development in a 30 s water bath and rinsed in another water bath. As the exposed dots which later were to become apertures are free standing pillars from the developer bath on, great care was taken not to expose them to unnecessary physical stress. Thus, samples were held in a horizontal orientation with the structures facing upwards when slowly taken out of one bath and into the next. The resulting aqueous meniscus on the surface avoided stressing the pillars with surface tension. Additionally, the meniscus prevented resist remains floating in the baths from drying in on the sample. After the third and last bath, samples were held horizontally and a gentle flow of water over the surface was established with a handheld washing bottle to rinse away any resist remains. Finally, the sample was dried in a controlled manner by turning it vertical. This let the meniscus withdraw slowly due to gravitational force.

**Metal deposition and lift-off:** Prior to metal evaporation, descumming of the samples was performed with a 200 W oxygen plasma for 180 s. A 100 nm thick aluminum film was then evaporated onto the sample in the above mentioned evaporator but with e-beam evaporation (acceleration voltage 8.5 kV,

emission current 50 mA) and a rate of 0.8 nm/s. Lift-off of the metal caps on the pillars, of the underlying resist pillars and the glass windows was done in a 5 min US-bath of 40 °C hot acetone. This was followed by 30 s baths in isopropanol and water. A final water rinse and a 120 s plasma clean cleared away possible remains of the lithography process. Samples were then stored under argon atmosphere until further use.

**Characterization:** Aperture diameters were measured after the experiments in the above mentioned electron microscope with a 5 nm Au layer sputtered (Sputter Coater S150B, Edwards) onto the previously cleaned samples to avoid charge accumulations in the apertures' glass bottoms (Fig. S2). AFM topography scans (Fig. S3) assured that our fabrication method resulted in steep sidewalls and a smooth glass bottom surface without resist remains. Scans were done on a commercial AFM-setup (MFP3D, Asylum Research) with a high aspect ratio cantilever probe (HART, Nanoscience Instruments) in tapping mode in air.

## Surface functionalization

To achieve better comparability to the stochastically immobilized probes, depot and target DNA were not immobilized via maleimide-sulfide bonds as in previous studies, but via biotin-avidin. This high-affinity bond withstands forces that are much higher than those of the SMC&P force hierarchy<sup>2</sup> and no significant decrease of transport efficiencies due to DNA-PEG rupture could be observed.

**Cleaning and chemically selective passivation of the aluminum surface:** After the described nanolithography and storage in argon, samples were cleaned in an US-bath of pure ethanol for 1 h, rinsed under water (water used for functionalization was MilliQ water) and sonicated again in water for 15 min. They were then blown dry by a nitrogen stream and subjected to a UV-cleaner (UVOH 150 Lab, FHR) for 30 min. In the following, they were immersed into a 90 °C hot aqueous solution (2% vol/vol) of polyvinylphosphonic acid (Polysciences) for 2 min, dipped in water for 20 s and carefully rinsed under water. Samples were then baked in an oven at 80 °C for 10 min. To further wash away physisorbed PVPA and to hydrolyze PVPA still bound to the glass surface, samples were then immersed in baths of, first water for 10 min, then methanol for 5 min and again water for 5 min, on a shaker (KS 260 basic, IKA). Gentle drying was done in a stream of nitrogen.

**Silanization and PEGylation:** Right after passivation samples were incubated in a freshly made solution of 3-aminopropyltrimethylethoxysilane (ABCR, Karlsruhe), water and ethanol (1:5:44, vol.:vol.) for one hour, dipped 10 times in each ethanol and water, and finally annealed in an 80 °C hot oven for 30 min. A freshly made 25 mM solution of NHS-PEG-biotin (3000 g/mol, Rapp) in sodium bicarbonate buffer (pH 8.3, 100 mM) was vortexed for 15 s and then centrifuged at 10,000 rpm for 30 s. Samples then were sandwiched in pairs with ZMW structures facing each other and 100 µl PEG-solution in between. After 3 hours incubation in a humid chamber, unbound PEG was washed off by 10 dips in beakers of each sodium bicarbonate buffer, water and again water. After gently drying with a nitrogen stream, samples were stored under argon until they were used in the stochastic experiments or further functionalized for SMC&P experiments, respectively.

## SMC&P functionalization

**Preparation of oligomeric DNA:** Sequences and labels of the used commercial DNA oligos (IBA) are listed in Table S1. First, transfer and depot DNA were hybridized in a thermocycler (Mastercycler gradient, Eppendorf) by heating up the 10  $\mu$ M mixture (ratio of 1:1) to 95 °C and then slowly cooling it down to 5 °C at a rate of 0.3 °C/s. Buffer was 1  $\times$  PBS. After that, neutravidin was pre-incubated with the depot/transfer-construct and the target DNA, respectively, at a concentration of 5  $\mu$ M and a ratio of 1:1, also in 1  $\times$  PBS. After one hour, DNA was further diluted to 1  $\mu$ M in 1  $\times$  PBS.

**Application of the microfluidic system:** Microfluidic polydimethylsiloxan (PDMS) channels were fabricated as described by Strackharn et al.<sup>3</sup>. Additionally, to reduce surface adhesion of the PDMS to the wafer and thus facilitate lift-off, the master mold wafer was exposed to perfluorodecyltrichlorosilane (97%, ABCR) vapor for 10 min before pouring the PDMS on. Also, care had to be taken to align the two channels with the target nanoapertures and the depot window, respectively. Thus, by-eye-alignment and contact were made with a mechanical xyz-microstage and the help of a stereo microscope.

**Assembly of depot and target area:** Target DNA and depot/transfer-construct were then sucked into the corresponding channels by a peristaltic pump (Gilson Minipuls 3) and incubated for 15 minutes. Unbound DNA was washed away with 200  $\mu$ l 1  $\times$  PBS flushed through the channels at a rate of 10  $\mu$ l/min. Finally, the PDMS channels were carefully removed in a bath of 1  $\times$  PBS to prevent neutravidin from falling dry and denaturing. Samples were then mounted into a teflon sample holder and buffer was exchanged with experimental buffer (50 mM MOPS, 150 mM potassium acetate, pH 7.1). Prior to experiments, the functionalization density was checked in a fluorescence microscope (Fig. S4).

**Alternative preparation with a microspotter:** We also successfully used an alternative approach and prepared depot and target areas by micro-structuring the PEGylated samples via a microspotter (GIX, Sonoplot)<sup>4</sup>. This represents a convenient approach to prepare multiple neighboring depots with different transfer constructs within the travel range of the AFM<sup>5</sup>. A standard glass capillary (World Precision Instruments) with an inner diameter of 30  $\mu$ m was used resulting in spots of a diameter of 45  $\mu$ m to 50  $\mu$ m on the cover glass (depot) and around 80  $\mu$ m on the metallic surfaces containing the apertures (target). Dispenser voltage was 2.5 to 3.8 V and dispensing time was 0.1 s. A humidity chamber with a moistening feedback held the humidity at 85% to improve the coupling density of DNA strands to the sample. Alignment of sample and glass capillary was achieved via the CCD camera of the microspotter. Depot and target areas were spotted with the same DNA-solutions that were incubated in the microfluidics system, and the sample was rinsed with 3 ml 1  $\times$  PBS after 15 minutes incubation time. Coupling densities on control samples were checked with a confocal scanner, they were comparable to those achieved with the microfluidic system.

## Cantilever preparation

Cantilevers were functionalized according to the recipe published in ref. 3. However, to be able to access the apertures we employed cantilevers with smaller tip radii and higher aspect ratios: Biolever Mini cantilevers (AC40TS, Olympus) with high aspect ratio silicon tips and MSCT cantilevers (Bruker) with silicon nitride tips. Their widths at a distance of 100 nm from the tip were measured by SEM (scanning electron microscopy) after sputtering them with 5 nm of Au for discharging purposes (Fig. S5). This width restricted us to use only Biolever Mini cantilevers in apertures of diameters smaller than 200 nm.

## Spectroscopy of stochastically immobilized dyes

Setup: Spectroscopic measurements of stochastically immobilized fluorophores were performed on a custom-built confocal microscope as described in ref. 6. An excitation wavelength of 640 nm was selected out of the broad emission spectrum of a pulsed supercontinuum laser (800MHz, Koheras SuperK Extreme, NKT Photonics) by an acousto-optic tunable filter (AOTF, AOTFnc-VIS, AA Optoelectronic). An inverse oil immersion objective (60x, NA 1.49, Apo N, Olympus) was used for excitation as well as for the collection of the fluorescence signal. The latter was separated from the majority of reflected laser light by a double band dichroic filter (Dualband z532/633 rpc, AHF Analysentechnik). Residual reflected light passing the dichroic was then separated from the fluorescence signal by a second dichroic filter (640 DCXR, AHF) and focused onto one of the two employed avalanche photodiodes (APD, SPCM-AQR-14, Perkin Elmer). This APD was protected from fluorescence by an emission filter (Brightline HC582/75, AHF) and provided the background signal used to identify nanoapertures. The fluorescence passing both dichroic filters was finally cleaned up by two emission filters (ET-Bandpass 700/75M and RazorEdge LP 647 RU, AHF) and focused onto the second APD. Two emission filters were used for this detection channel to minimize background from metallic reflection. The detection signal was synchronized with the pulsed laser excitation and collected by a time-correlated single photon counting card (Hydra Harp 400, PicoQuant) which measures the specific lifetime  $\Delta t$  of each detected photon<sup>7</sup>.

**Immobilization:** For comparability with SMC&P placed probes, we used a double-stranded DNA oligo consisting of Atto647N-labeled transfer and biotinylated target strand. The construct was hybridized and pre-incubated with neutravidin in the same manner as the depot construct described above. Under steady state optical control, probes were incubated until reasonable ratios of occupied apertures (~20 %) were obtained. The loading buffer was 1 × PBS and the corresponding concentrations and incubation times for the different aperture sizes were: 50 pM and 2 min for the glass reference dyes and those immobilized in 750 nm diameter apertures, 100 pM and 15 min for the 375 nm apertures and 300 pM and 25 min for the apertures with 150 nm diameters. Five consecutive buffer exchanges with experimental buffer (see next section) stopped immobilization and extracted unbound probes from the sample.

**Measurement:** To reduce the risk of corrosion<sup>8</sup>, the actual confocal measurements were performed with a chloride-free experimental buffer (pH 7.1) of 50 mM MOPS, 150 mM potassium acetate, 1 mM of ascorbic acid and methylviologen. The latter two were freshly solved from powder and they served as reducing and oxidizing system (ROXS)<sup>9</sup> to reduce the lifetime of the non-fluorescent triplet state thus stabilizing the dyes' fluorescence signal. It is worth noting that the stochastic data presented in this work was recorded during one single experiment and performed on the same sample. The experiment started with confocal scans of the glass reference dyes immobilized in the large depot window of our sample structure. It was then proceeded with scanning of the apertures, starting with large diameters and finishing with the small ones. After all apertures of one size had been recorded, additional incubation according to the next aperture size was done before proceeding with the next set of confocal scans. After each confocal scan, the ~15% most intense dyes were additionally probed by recording a fluorescence transient. Investigation of the stepwise photobleaching in the transients allowed exclusion of data from double- or even triple-occupations.

**Data analysis:** The fluorescence properties of specific dyes in the confocal scans were then analyzed by custom-made software (LabView): A spot finding algorithm extracted the photons from one detected dye. The lower relative intensity threshold at which dyes were to dim to be detected was at ~20% of the mean intensity of the glass reference dyes. The amount of photons denoted to one dye directly determined its intensity. For lifetime analysis, the delay times of these photons were added up to a fluorescence decay which was fit by a commercial deconvolution software (Fluofit, PicoQuant). To achieve lifetime resolution below 1 ns, this software fits a monoexponential decay, reconvoluted with the instrument's response function (IRF), to the recorded fluorescence decays. An exemplary fluorescence decay curve with the IRF and a reconvoluted fit is shown in Fig. S6. The IRF of our confocal microscope was measured from scattered laser light, and care was taken so that the intensity during IRF-recordings was of comparable magnitude to the fluorescence intensities of the dyes. A further important advantage of the deconvolution software is that varying background scattering e.g. by the aluminum cladding of the apertures can be compensated by one fit parameter of the decay.

## TIRF / Confocal / AFM Hybrid Microscope Setup

Loading of the nanoapertures by means of SMC&P and the consecutive lifetime measurements were performed on a custom-built setup combining atomic force microscopy with confocal as well as total internal reflection fluorescence (TIRF) microscopy. It is thus a further development of the TIRF/AFM-hybrid setup described in ref. 10. It is schematically depicted in Fig. S7.

**Confocal:** For the confocal part of the instrument a pulsed supercontinuum laser (Koheras SuperK Extreme, NKT Photonics), restricted to 640 nm with an AOTF (AOTFnc-VIS, AA Optoelectronic) and cleaned up by a filter (HQ 640/10, AHF), served as excitation source. The laser beam was reflected into a high numerical aperture objective (60x, NA 1.49, Apo N, Olympus) by a dichroic filter (Dualband z532/633 rpc, AHF) and focused onto the specimen. Fluorescence was collected through the same objective passed the dichroic as well as an IR-blocking filter (HC 750/SP, AHF), and was focused onto

a pinhole (50  $\mu\text{m}$ ) by a tubus lens (U-TLU, Olympus). A system of two additional lenses ( $f = 150 \text{ mm}$ ,  $f = 25 \text{ mm}$ ) focused fluorescence light passing the pinhole onto an APD (SPCM-AQR-14, Perkin Elmer) that was protected by two fluorescence emission filters (ET-Bandpass 700/75M and RazorEdge LP 647 RU, AHF). Pulse repetition rate, photon counting system and measuring software were the same as in the confocal microscope used for the stochastic measurements. However, confocal scanning was done by movement of the objective via a xyz-piezo (Physik Instrumente).

**TIRF:** Switching to the combined TIRF microscope was done with two motorized flip mirrors as depicted in the schematics (Fig. S7). The TIRF laser source, a 638 nm continuous wave laser (Cube 1064915, Coherent), was cleaned up with a laser filter (BrightLine HC 636/8, AHF). Fluorescence was collected through the objective, passed the dichroic filter, was cleaned up by an emission filter (M 700/75, AHF) and focused onto an EMCCD (iXon 512x512, DU-897, Andor). The overall resolution of the TIRF-system was 102 nm/pixel. The camera chip was operated at a temperature of  $-75 \text{ }^\circ\text{C}$  and an electron multiplication gain of 300 was applied.

**AFM:** The AFM head did only differ in one aspect from the one described ref. 10: For extraordinary transmission localization, three LEDs were mounted to the AFM-head as white light illumination source. A stable table (Micro40 M6/25, HALCYOICS) required for reducing vibrational noise in the AFM-signal was implemented underneath the main parts of the setup in such a way that the optical paths of confocal and TIRF fluorescence would leave it as parallel beams (see Fig. S7). This decoupled parallel movement of the stable table from optical signals. The AFM was controlled via self-written IGOR software (Wavemetrics), and cantilever calibration was based on the equipartition theorem<sup>11</sup>. For SMC&P processes, the sample was moved relative to the AFM by a xy-piezo stage (Physik Instrumente). An additional software routine allowed the external triggering of force curves i.e. cut and paste events via an analog signal.

**Software:** A custom-made software (LabView) was used to control TIRF laser, LED illumination, the sample holding xy-piezo and the EMCCD camera. The software also had the Gaussian fitting routines implemented and triggered the cut and paste routines by signaling to the AFM software. The main steps of the aperture loading procedure were executed by automated routines of the software. This was necessary to minimize the time lag between localization of the active anchor and the subsequent loading of an aperture, thus minimizing inaccuracies caused by thermal drift of involved components. To allow accurate conversion of the optically measured relative movements into piezo positions, the x- and y- conversion factors and a rotational constant were measured in a calibration procedure. For this, an aperture was localized optically, moved with the piezos by a known distance and then localized again.

## SMC&P procedure

Whereas the lifetime measurements of pasted dyes were conducted on the setup described above, the loading process presented in Fig. 3 was made on another setup. It is described in ref. 8 and

equipped with a green TIRF laser (532 nm wavelength). This is why a Cy3b label was used instead of the ATTO647N on the transfer strand.

**Localization of the active anchor:** Broad alignment of cantilever, sample and optics was done by eye under white light transmission and approximate positions of depot, reference window and target were saved. Loading of an aperture was then started by loading a transfer molecule from the depot onto the cantilever and pasting it into the reference window nearby the apertures. This process was optically controlled in TIRF illumination. Upon pasting and retraction of the cantilever, the dye was localized in an EMCCD image by a 2D-Gaussian fitting algorithm and its coordinates within the camera's coordinate system were saved. As the cantilever is kept at a fixed position with respect to the optical axis and the sample is moved instead, this position of the cantilever within the camera image is fixed.

**Loading of the aperture:** The aperture to be loaded was then positioned roughly underneath the cantilever by eye and localized with a Gaussian fit in LED illumination. The relative movement determined by the conversion factors and the localizations of the two fits was typically at the order of one micrometer, which reduced possible errors from imprecision of the conversion factors. After equipping the cantilever with a new transfer molecule from the depot, it was aligned with the aperture, and a paste in the aperture center was made. All cut- and paste processes were controlled live by TIRF fluorescence and force-distance curves.

**Comparability:** For lifetime measurements of pasted dyes, the same experimental buffer as in the stochastic measurements was used. Confocal scans were made right after loading of each aperture. To assure reproducible focusing of the confocal beam onto the surface plane and thus comparability of the fluorescence intensities, fine-adjustment of objective-sample distance was made in TIRF mode. To allow comparison of data from the two different confocal instruments (hybrid and regular), confocal scans of reference fluorophores pasted into a glass window were used for normalization.

## Calculation of the loading process's lateral uncertainty

There are four main sources for lateral uncertainty in our aperture loading procedure: The positioning uncertainty of the two pastes (reference paste and final loading of the aperture) and the errors of the two superresolution localizations.

To measure the optical localization precision of our instrument, we carried out 100 subsequent localizations of a single dye under the same experimental conditions as in the SMC&P experiments (Fig. S8). The localizations were made on single frames of 0.1 s acquired over 10 s. Each frame had collected  $990 \pm 110$  fluorescence photons from the dye, which corresponds well with the range of photon counts used for localizations of the reference pastes in the SMC&P experiments. The resulting standard error of the 100 localized positions was 9.7 nm. According to ref. 12, this localization

precision can be approximated by  $\frac{s}{\sqrt{N}}$ , where  $s$  is the standard deviation of the point spread function

and  $N$  is the number of detected photons. An additional prefactor of  $\sqrt{2}$  is necessary to take account for EMCCD excess camera noise<sup>13</sup>. With  $s = 280 \pm 3$  nm for the used setup, the theoretical localization precision for 990 photons thus is: 6.3 nm. This discrepancy between theory and experiment can be explained by polarization effects<sup>14</sup>.

Other than fluorescence from dyes, extraordinary transmission of nanoapertures is not limited by photobleaching. Therefore, we collected at least a fourfold amount of photons from them. In the case of the less transmissive zero-mode waveguides, this was achieved by maximizing the LED emission power and by raising the integration time. The error of localizing a nanoaperture can therefore be approximated with 4.9 nm.

Regarding the general accuracy of a SMC&P event, we have previously demonstrated that the precision by which single molecules are placed relative to one another is  $\pm 11$  nm<sup>15</sup>.

Therefore, the overall precision of our method - approximated by twice the uncertainty of a paste plus the localization errors of one dye and one aperture - sums up to 19 nm. It is dominated by the general positioning uncertainty of single SMC&P pastes, which could be reduced by shorter linker lengths or by denser surface functionalization<sup>15</sup>. This error analysis takes into account that the time interval between reference paste and loading of an aperture was less than 20 s, allowing to neglect the drifts of cantilever and sample.

## References

1. Foquet, M.; Samiee, K. T.; Kong, X.; Chauduri, B. P.; Lundquist, P. M.; Turner, S. W.; Freudenthal, J.; Roitman, D. B. *J. Appl. Phys.* **2008**, 103, (3), 034301.
2. Moy, V.; Florin, E.; Gaub, H. E. *Science* **1994**, 266, (5183), 257-259.
3. Strackharn, M.; Stahl, S. W.; Puchner, E. M.; Gaub, H. E. *Nano Lett.* **2012**, 12, (5), 2425-2428.
4. Severin, P. M. D.; Gaub, H. E. *Small* **2012**, 8, (21), 3269-3273.
5. Strackharn, M.; Stahl, S. W.; Severin, P. M. D.; Nicolaus, T.; Gaub, H. E. *ChemPhysChem.* **2011**, 13, (4), 914-917.
6. Stein, I. H.; Capone, S.; Smit, J. H.; Baumann, F.; Cordes, T.; Tinnefeld, P. *ChemPhysChem.* **2011**, 13, (4), 931-937.
7. Acuna, G. P.; Bucher, M.; Stein, I. H.; Steinhauer, C.; Kuzyk, A.; Holzmeister, P.; Schreiber, R.; Moroz, A.; Stefani, F. D.; Liedl, T.; Simmel, F. C.; Tinnefeld, P. *ACS Nano* **2012**, 6, (4), 3189-3195.
8. Heucke, S. F.; Stahl, S. W.; Puchner, E. M.; Holleitner, A. W.; Tinnefeld, P.; Gaub, H. E. *Int. J. Nanotechnol. (in the press)*.
9. Vogelsang, J.; Kasper, R.; Steinhauer, C.; Person, B.; Heilemann, M.; Sauer, M.; Tinnefeld, P. *Angew. Chem. Int. Ed.* **2008**, 47, (29), 5465-5469.
10. Gump, H.; Stahl, S. W.; Strackharn, M.; Puchner, E. M.; Gaub, H. E. *Rev. Sci. Instrum.* **2009**, 80, (6), 063704 (5).
11. Butt, H. J.; Jaschke, M. *Nanotechnology* **1995**, 6, 1-7.
12. Thompson, R. E.; Larson, D. R.; Webb, W. W. *Biophys. J.* **2002**, 82, (5), 2775-2783.
13. Bossi, M.; Fölling, J.; Belov, V. N.; Boyarskiy, V. P.; Medda, R.; Egner, A.; Eggeling, C.; Schönle, A.; Hell, S. W. *Nano Lett.* **2008**, 8, (8), 2463-2468.
14. Enderlein, J.; Toprak, E.; Selvin, P. R. *Opt. Express* **2006**, 14, (18), 8111-8120.

15. Kufer, S. K.; Strackham, M.; Stahl, S. W.; Gump, H.; Puchner, E. M.; Gaub, H. E. *Nat. Nanotechnol.* **2008**, 4, (1), 45-49.

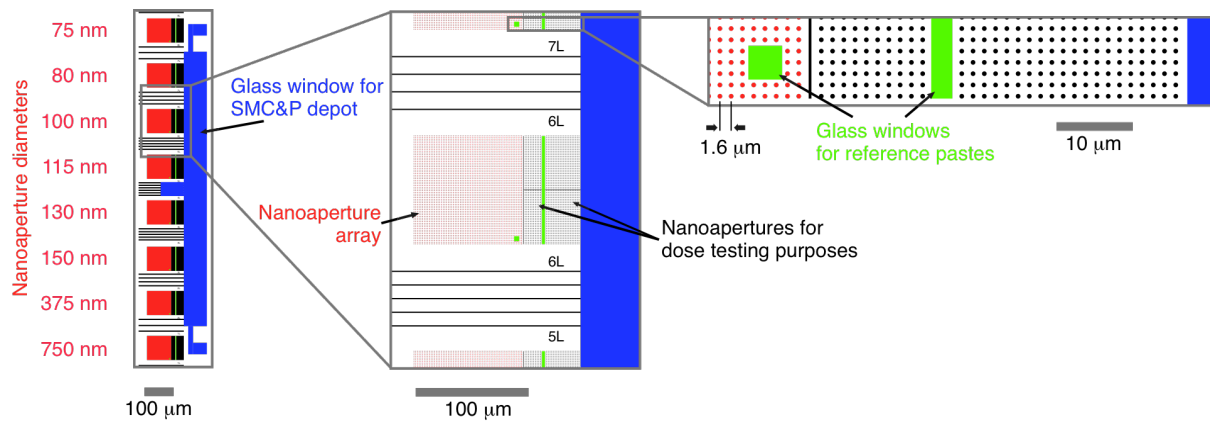


**Fig. S1.** Drawing of the lithography pattern: The large quadratic fields (red) are aperture arrays of different aperture diameters. The large blue vertical rectangle represents the depot glass window. In between aperture arrays and depot, dose tests were written to control the quality of our fabrication process. The small green areas are glass windows for reference pastes.

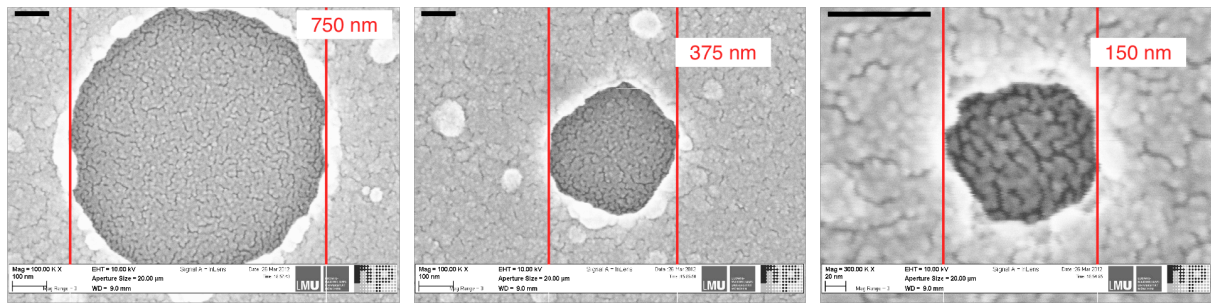


**Fig. S2.** SEM images of the different size nanoapertures: The fine texture in the scans originates from a 5 nm gold film sputtered onto the samples to avoid charge accumulations in the apertures' glass bottoms. The black bars in the top left corners represent 100 nm.

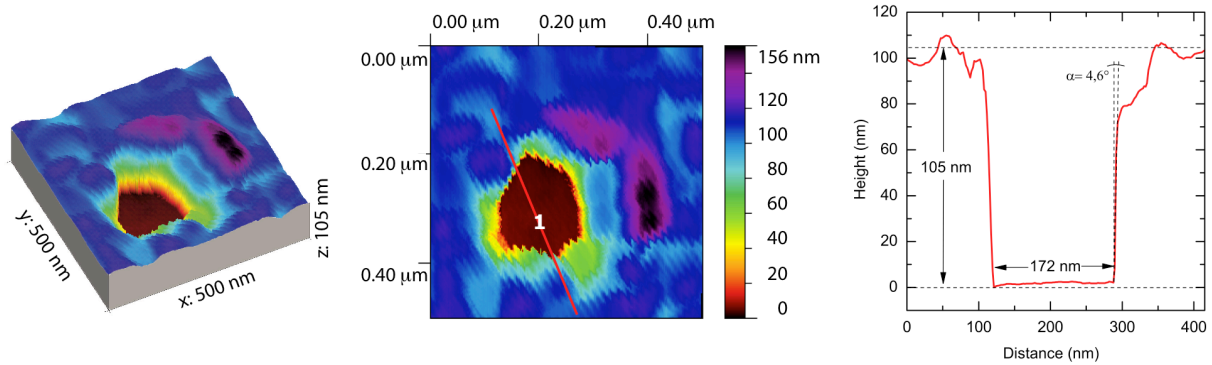


**Fig. S3.** AFM topography scan of a 175 nm diameter aperture: It features a smooth glass surface and steep sidewalls. The sidewall angle measured in the cross section represents the apex angle of the used high aspect ratio cantilever tip.

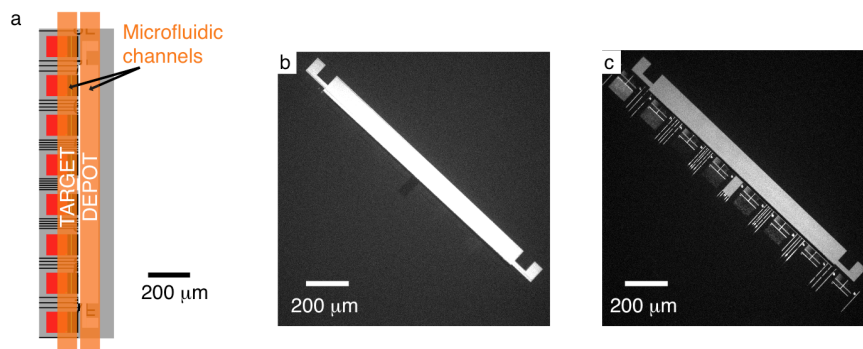


**Fig. S4.** SMC&P functionalization: (a) Schematic drawing indicating the position and the orientation of the microfluidic channels relative to the sample structure. (b) Fluorescence from the ATTO647N labeled transfer strand in the depot region. (c) Fluorescence of an avidin label (Alexa Fluor 488) present in both, depot and target region.

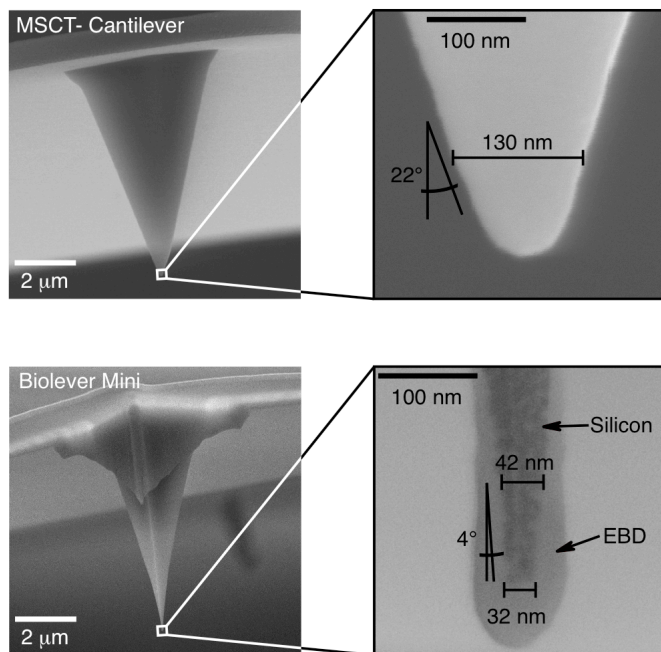


**Fig. S5.** SEM micrographs of the two cantilever types used in the experiments: Width and apex angle at 100 nm distance from the tips are plotted in close up. The grey layer around the silicon tip of the Biolever Mini in the close up is an artifact from SEM imaging (electron beam deposition layer, EBD) and no intrinsic part of the cantilever.

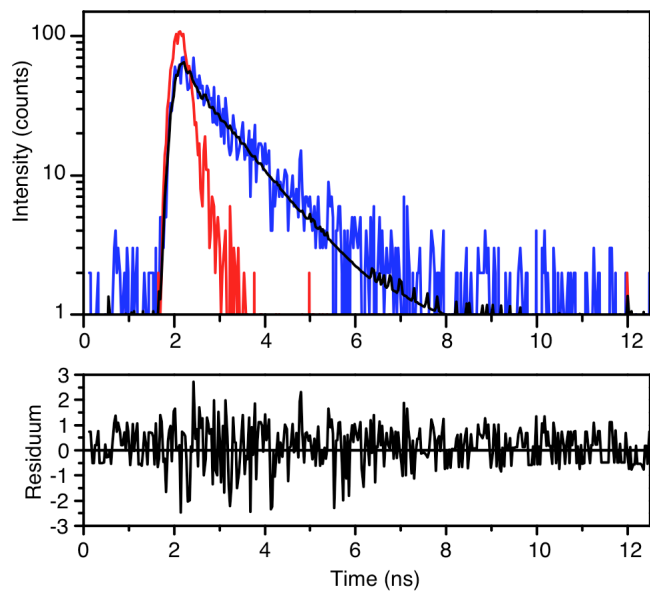


**Fig. S6.** Fluorescence lifetime fit: The fluorescence decay of a single fluorophore immobilized in a nanoaperture is shown in blue and the impulse response function in red. The reconvolving fit (black) matches the fluorescence decay. The resulting residuum is shown below.

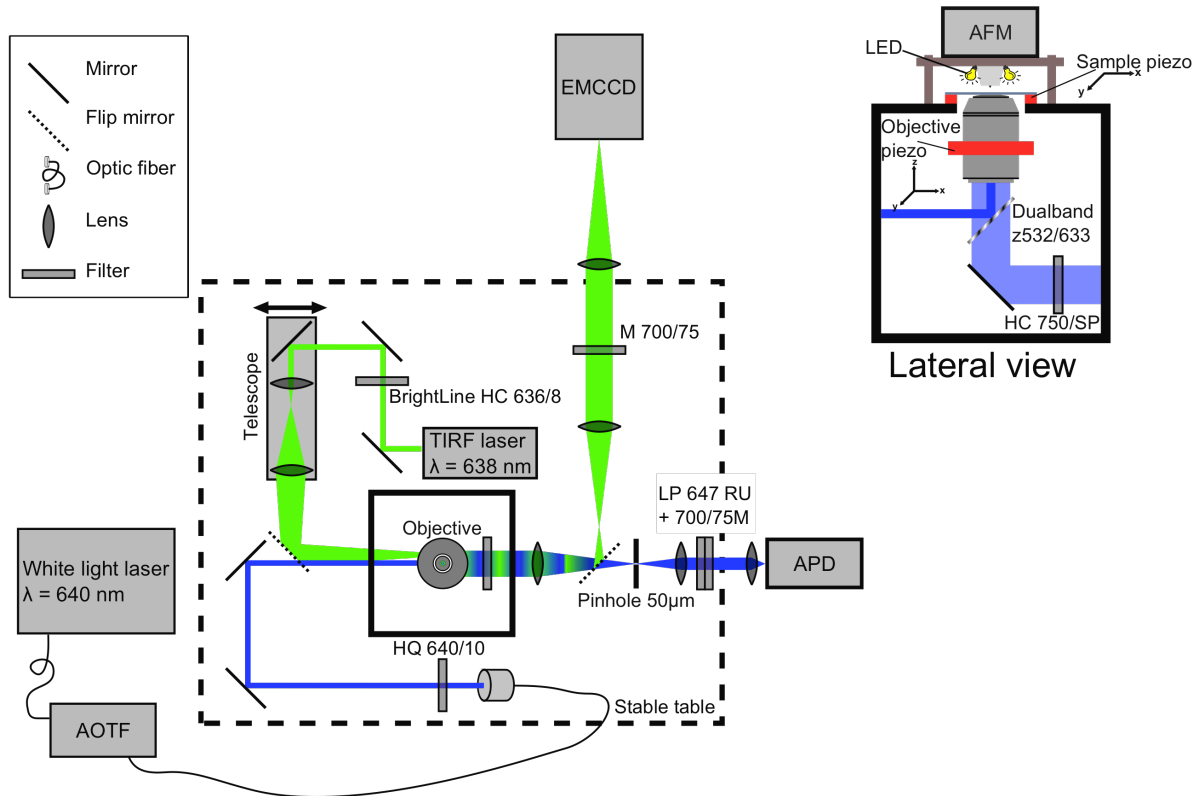


**Fig. S7.** Schematics of the TIRF / Confocal / AFM Hybrid Microscope Setup: The green path represents the excitation and emission in the total-internal reflection fluorescence (TIRF) microscopy mode. In blue, the path of confocal laser excitation and detection is shown. In transmission mode, laser sources are blocked and light emitting diodes (LEDs, drawn in the lateral view) on the AFM head are used as excitation source. In this mode, the EMCCD camera detects a dominantly red fraction of the LEDs' emission spectrum since all detected light has to pass the dualband dichroic filter as well as the emission filter in front of the camera.

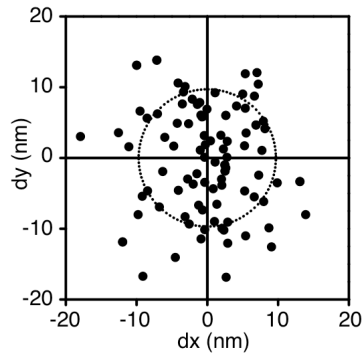


**Fig. S8.** Superresolution accuracy of the setup: 100 subsequent localizations of the same fluorophore result in a standard deviation of 9.7 nm (dotted circle). Localizations were made by Gaussian fits on approx. 1000 photons each.

Table S1. Sequences of the partially thiolated (SH) or biotinylated DNA oligos used.

Depot	5' (Biotin) TTTTAAAGTAGCTATTCGAACTATAGCTTAAGGACGTCAA 3'
Transfer	5' TTGACGTCCTT (Atto647N) AAGCTATAGTTCGAATAGCTACTTTTTGATATCGAATTCCTGCAGTT 3'
AFM	5' SH- TTTT CTGCAGGAATTCGATATCAA 3'
Target	5' AAAAAGTAGCTATTCGAACTATAGCTTAAGGACGTCTTTTTTTTT (Biotin) 3'